Quasiparticle interference in iron-based superconductors

A. Akbari,[1] J. Knolle,[2] I. Eremin,[1] and R. Moessner[2]

[1]*Institut für Theoretische Physik III, Ruhr-Universität Bochum, D-44801 Bochum, Germany*
[2]*Max Planck Institute for the Physics of Complex Systems, D-01187 Dresden, Germany*

We systematically calculate quasiparticle interference (QPI) signatures for the whole phase diagram of iron-based superconductors. Impurities inherent in the sample together with ordered phases lead to distinct features in the QPI images that are believed to be measured in spectroscopic imaging-scanning tunneling microscopy. In the spin-density wave phase the rotational symmetry of the electronic structure is broken, signatures of which are also seen in the coexistence regime with both superconducting and magnetic order. In the superconducting regime we show how the different scattering behavior for magnetic and nonmagnetic impurities allows to verify the s^{+-} symmetry of the order parameter. The effect of possible gap minima or nodes is discussed.

I. INTRODUCTION

The relation between unconventional superconductivity (SC) and magnetism is one of the most interesting topics in condensed-matter physics. In iron-based superconductors[1] this question is of particular interest because in some of these systems such as $Ba(Fe_{1-x}Co_x)_2As_2$ and $SmFeAs(O_{1-x}F_x)$, SC, and *metallic* antiferromagnetism (AFM) coexist homogeneously.[2,3] This coexistence is characterized by a competition of the two ordered states which results in a dramatic suppression of the magnetization below the SC transition temperature, T_c, to the extent that re-entrance of the nonmagnetically ordered superconducting phase sets in at low temperatures.[4]

A number of groups have argued[5–9] that in the ferropnictides (FPs), the same electrons contribute to the superconducting condensate and to the formation of the ordered magnetic moment. Furthermore, it was shown[4,8,9] that a coexistence of the two phases occurs only for a large set of parameters when the superconducting order is of the s^{+-} type, i.e., the superconducting gap changes sign between hole and electron Fermi-surface pockets which are located around the Γ and $(\pm\pi, 0)$, $(0, \pm\pi)$ points of the Brillouin zone (BZ) based on one Fe ion per unit cell (so-called *unfolded* BZ). Therefore, a large coexistence region in the phase diagram of FPs indirectly supports the s^{+-}-wave symmetry of the SC order in these systems.

The AFM [or spin-density-wave (SDW)] phase itself shows a number of interesting properties which still have not been completely understood. Given the electronic structure of FPs, consisting of two hole and two electron Fermi-surface pockets located around the Γ and $(\pm\pi, 0)$, $(0, \pm\pi)$ points of the BZ,[10] it is natural to assume that AFM order emerges, at least partly, due to near nesting between the dispersions of holes and electrons.[5,6,11–19] Within this scenario the selected magnetic order is either with momentum $\mathbf{Q}_1 = (\pi, 0)$ or $\mathbf{Q}_2 = (0, \pi)$ (Ref. 7) which corresponds to ferromagnetic order along one and antiferromagnetic order along the other direction. The collective spin excitations in the ordered state reveal pronounced anisotropy along x and y directions which is a consequence of the fact that only one of the two elliptic pockets is involved in the formation of the AFM state.[20] Similarly, the electronic structure in the AFM ordered state is anisotropic and the quasiparticle interference (QPI) introduced by scalar nonmagnetic, as well as magnetic, impurities gives rise to a pronounced quasi-one-dimensional (1D) periodic modulation of the real-space local density of states (LDOS) which, as we argued in Ref. 21, is in agreement with spectroscopic imaging-scanning tunneling microscopy (SI-STM) experiments in $Ca(Fe_{1-x}Co_x)_2As_2$.[22]

Overall, QPI has become a powerful experimental tool for elucidating the nature of the many-body states in novel superconductors. In the presence of impurities, elastic-scattering mixes two quasiparticle eigenstates with momenta $\mathbf{k}_1$ and $\mathbf{k}_2$ on a contour of constant energy. The resulting interference at wavevector $\mathbf{q} = \mathbf{k}_2 - \mathbf{k}_1$ reveals a modulation of the LDOS. The interference pattern in momentum space can be visualized by means of the SI-STM.[23] In layered cuprates the analysis of the QPI has provided details of the band structure, the nature of the superconducting gap, or other competing orders.[24–27]

In the superconducting state of iron-based superconductors a recent SI-STM experiment claimed to unambiguously identify the order-parameter symmetry to be of the s^{+-} character.[28] Theoretical analyzes performed previously have also shown a pronounced difference in interference patterns characteristic of a simple s-wave symmetry and an extended s^{+-}-wave symmetry (see Refs. 29–32). In particular, in the presence of vortices an additional source of scattering either suppresses or enhances intrapocket and interpocket scatterings depending on the symmetry of the superconducting gap,[30] a feature found also in the experimental data.[28] At the same time, the experimental results have been put into question and argued instead to arise from the Bragg scattering and not due to QPI.[33]

In what follows we address signatures of the different orders on the electronic structure as seen in the distinctive features probed by QPI. In particular, we extend our previous analysis of the QPI in the AFM state[21] to the entire phase diagram of the FPs assuming that the AFM and SC arise from the same quasiparticles. We present the results for QPI in the coexistence regime of AFM+SC with s- and extended s-wave (s^{+-}) symmetry as well as for the pure superconduct-

ing state. We further investigate the role of higher harmonics (nontrivial angular dependence along the Fermi surface) in the extended *s*-wave case and, in particular, we address the question whether a nodeless or nodal s^{+-}-wave symmetry can be identified within SI-STM. The aim of our analysis is to find subtle features of the various many-body states in iron-based superconductors that can be probed by STM.

The paper is organized as follows. The theoretical calculations to obtain the LDOS are based on a four band model and they are explained in Sec. II. Based on our model we numerically analyze the QPI signatures in the various phases in Sec. III. We conclude the paper by a summary (Sec. IV).

II. THEORETICAL MODEL

We employ an effective mean-field four band model with two circular hole pockets centered around the (0,0) point of the unfolded BZ (α bands) and two elliptic electron pockets centered at $(\pm\pi, 0)$ and $(0, \pm\pi)$ points of the BZ, respectively, (β bands) (Ref. 20)

$$H_c = \sum_{\mathbf{k},\sigma,i=\alpha_1,\alpha_2,\beta_1,\beta_2} \varepsilon_{\mathbf{k}}^i c_{i\mathbf{k}\sigma}^\dagger c_{i\mathbf{k}\sigma} + \sum_{\mathbf{k},\sigma,i=\alpha_1,\alpha_2,\beta_1,\beta_2} [\Delta_{\mathbf{k}}^i c_{i\mathbf{k}\sigma}^\dagger c_{i-\mathbf{k}-\sigma}^\dagger$$

$$+ \text{H.c.}] + \sum_{\mathbf{k}\sigma} W\sigma[c_{\alpha_1\mathbf{k}\sigma}^\dagger c_{\beta_1\mathbf{k}+\mathbf{Q}_1\sigma} + \text{H.c.}]. \quad (1)$$

Here, we set the electronic dispersions to $\varepsilon_{\mathbf{k}}^{\alpha_i} = \varepsilon_0 + t_\alpha(\cos k_x + \cos k_y) - \mu_i$, $\varepsilon_{\mathbf{k}}^{\beta_1} = \varepsilon_0 + t_\beta[[1+\epsilon]\cos(k_x+\pi) + [1-\epsilon]\cos(k_y)] - \mu_1$, and $\varepsilon_{\mathbf{k}}^{\beta_2} = \varepsilon_0 + t_\beta[[1-\epsilon]\cos(k_x) + [1+\epsilon]\cos(k_y+\pi)] - \mu_1$. ϵ accounts for the ellipticity of the electron pockets. Following our previous analysis of the spin excitations and QPI in the magnetically ordered state, we use Fermi velocities and size of the Fermi pockets based on Ref. 10, namely, $t_\alpha = 0.85$ eV, $t_\beta = -0.68$ eV, $\mu_{\alpha_1} = 1.54$ eV, $\varepsilon_0 = 35$ meV, $\mu_{\alpha_2} = 1.44$ eV, $\mu_1 = -1.23$ eV, and $\epsilon = 0.5$. For these values, the Fermi velocities are 0.5 eV a for the α_1 band, where a is the lattice spacing, and $v_x = 0.27$ eV a and $v_y = 0.49$ eV a along x and y directions for the β_1 band, and vice versa for β_2. We use $a_x = a_y = a = 1$.

Here, $\Delta_{\mathbf{k}}^i$ is the superconducting gap for band i. Symmetry and structure of the superconducting gap in Fe-based superconductors have been subject of numerous experimental and theoretical papers in recent years.[1,5,6,10–12,31,32,34–37] There is a growing consensus that the gap has an extended *s*-wave symmetry—it belongs to a symmetric A_{1g} representation of the D_{4h} symmetry group of a square lattice. Gap values along electron and hole Fermi surfaces (FSs) are of opposite signs.

A more subtle issue is whether the gap has nodes. This is not a symmetry issue as adding higher harmonics to the extended *s*-wave gap yields stronger momentum dependence of the latter on the FS. Quite generally one can write the superconducting gap in the form

$$\Delta_{\mathbf{k}} = \Delta[\cos k_x \cos k_y] + \Delta'[\cos(k_x) + \cos(k_y)]/2. $$

For $\Delta' = 0$ the superconducting gap can be roughly approximated by a constant on the hole and electron FS pockets but with opposite signs, $\Delta^e = -\Delta^h \simeq -\Delta$. Increasing Δ' does not significantly change the momentum dependence of the gap on the FS of the hole pockets which can be approximated as

$\Delta^{\alpha_i} = \Delta^h$ while it introduces substantial angular dependence of the superconducting gap on the electron pockets in the form $\Delta^{\beta_i}(\psi) = \Delta^e(1 \pm b\cos 2\phi)$. Here, ϕ is the angle measured from the line connecting the two electron FSs, i.e., the line between $(\pi, 0)$ and $(0, \pi)$ points of the first BZ and $b \simeq 2\Delta'/\Delta$. Such $\Delta^{\beta_i}(\phi)$ has no nodes if $b < 1$ but "accidental" nodes do appear when $b > 1$. Their positions are determined by $\cos 2\phi = 1/b$ and the latter shift continuously with b so that the node's location is not selected by any symmetry.

FPs are multiorbital systems and the orbital nature of the quasiparticle states introduces a sizable variation in the interaction along the Fermi surface. This manifests itself as a $\cos 2\phi$ component of the interaction. In particular, b grows upon inclusion of the intraband Coulomb repulsion into the gap equation because this term couples to the gap averaged over the FS and hence reduces angle-independent gap components but does not affect $\cos 2\phi$ components (Refs. 5, 6, 36, and 37). As a consequence, b becomes progressively larger as the system moves further away from the SDW phase and the effect of intraband repulsion grows. In other words overdoped FPs are more likely to have nodes in the gap.

We introduce the experimentally observed $(\pi, 0)$ SDW order parameter, within a standard mean-field approximation: $\vec{W} \propto \sum_{\mathbf{p}} \langle c_{\alpha_1\mathbf{p}\delta}^\dagger c_{\beta_1\mathbf{p}+\mathbf{Q}_1\gamma} \vec{\sigma}_{\delta\gamma} \rangle$. In this state, one of the α fermions couples with only one band of β fermions, leaving the other hole and electron bands—and hence their electron and hole FSs—unaffected by the SDW. Without loss of generality we direct $\vec{W}$ along the z-quantization axis.

The actual QPI which is believed to be measured in SI-STM (Ref. 23) arises from quasiparticle scattering by perturbations internal to the sample such as nonmagnetic or magnetic impurities. We perform a standard analysis of such processes based on a T-matrix description.[38] In particular, we introduce an impurity term in the Hamiltonian

$$\mathcal{H}_{imp} = \sum_{\mathbf{k}\mathbf{k}'ii'\sigma\sigma'} (V_{\mathbf{k}\mathbf{k}'}^{ii'}\delta_{\sigma\sigma'} + J_{\sigma\sigma'}^{ii'}\mathbf{S}\cdot\sigma_{\sigma\sigma'})c_{i\mathbf{k}\sigma}^\dagger c_{i'\mathbf{k}'\sigma'}, \quad (2)$$

where $V_{\mathbf{k}\mathbf{k}'}^{ii'}$ and $J_{\sigma\sigma'}^{ii'}$ represent the nonmagnetic and the magnetic pointlike scattering between the electrons in the bands i, and i' respectively. In the following we set the quantization axis of the magnetic impurity along the z direction. Following Ref. 38, we define the new Nambu spinor as $\hat{\psi}_{\mathbf{k}}^\dagger = (c_{\alpha_2\mathbf{k}\uparrow}^\dagger, c_{\alpha_1\mathbf{k}\uparrow}^\dagger, c_{\beta_1\mathbf{k}\uparrow}^\dagger, c_{\beta_2\mathbf{k}\uparrow}^\dagger, c_{\alpha_2-\mathbf{k}\downarrow}, c_{\alpha_1-\mathbf{k}\downarrow}, c_{\beta_1-\mathbf{k}\downarrow}, c_{\beta_2-\mathbf{k}\downarrow})$, where now we measure the momentum-transfer relative to the interpocket momentum $\mathbf{k}+\mathbf{Q}_1$, e.g., $c_{\beta_1\mathbf{k}+\mathbf{Q}_1\sigma}$. Therefore, the Hamiltonian can be written as

$$\mathcal{H} = \sum_{\mathbf{k}} \hat{\psi}_{\mathbf{k}}^\dagger \hat{\beta}_{\mathbf{k}} \hat{\psi}_{\mathbf{k}} + \sum_{\mathbf{k}\mathbf{k}'} \hat{\psi}_{\mathbf{k}}^\dagger \hat{U}_{\mathbf{k}\mathbf{k}'} \hat{\psi}_{\mathbf{k}'}, \quad (3)$$

where by defining $V_{\mathbf{k}\mathbf{k}'}^{ii} = \gamma u_0$; $V_{\mathbf{k}\mathbf{k}'}^{ii'} = \gamma u_Q$ and $J_{zz}^{ii}S_z = \gamma' u_0$; $J_{zz}^{ii'}S_z = \gamma' u_Q$, the matrices $\hat{\beta}_{\mathbf{k}}$ and $\hat{U}_{\mathbf{k}\mathbf{k}'}$ are defined as

$$\hat{\beta}_{\mathbf{k}} = \begin{bmatrix} \hat{\varepsilon}_{\mathbf{k}}^{\uparrow} & \hat{\Delta}_{\mathbf{k}} \\ \hat{\Delta}_{\mathbf{k}} & \hat{\varepsilon}_{\mathbf{k}}^{\downarrow} \end{bmatrix}; \quad \hat{U}_{\mathbf{k}\mathbf{k}'} = \begin{bmatrix} \gamma' + \gamma & 0 \\ 0 & \gamma' - \gamma \end{bmatrix} \otimes \hat{I}_{\mathbf{k}\mathbf{k}'}.$$

$\otimes$ is the direct product of matrices and

$$\hat{\varepsilon}_{\mathbf{k}}^{\sigma} = \sigma \begin{bmatrix} \varepsilon_{\mathbf{k}}^{\alpha_2} & 0 & 0 & 0 \\ 0 & \varepsilon_{\mathbf{k}}^{\alpha_1} & \sigma W & 0 \\ 0 & \sigma W & \varepsilon_{\mathbf{k}}^{\beta_1} & 0 \\ 0 & 0 & 0 & \varepsilon_{\mathbf{k}}^{\beta_2} \end{bmatrix};$$

$$\hat{\Delta}_{\mathbf{k}} = \begin{bmatrix} \Delta_{\mathbf{k}}^{\alpha_2} & 0 & 0 & 0 \\ 0 & \Delta_{\mathbf{k}}^{\alpha_1} & 0 & 0 \\ 0 & 0 & \Delta_{\mathbf{k}}^{\beta_1} & 0 \\ 0 & 0 & 0 & \Delta_{\mathbf{k}}^{\beta_2} \end{bmatrix};$$

$$\hat{I}_{\mathbf{k}\mathbf{k}'} = \begin{bmatrix} u_0 & u_0 & u_{\mathbf{Q}} & u_{\mathbf{Q}} \\ u_0 & u_0 & u_{\mathbf{Q}} & u_{\mathbf{Q}} \\ u_{\mathbf{Q}} & u_{\mathbf{Q}} & u_0 & u_{\mathbf{Q}} \\ u_{\mathbf{Q}} & u_{\mathbf{Q}} & u_{\mathbf{Q}} & u_0 \end{bmatrix}.$$

The spin index is $\sigma = \pm 1$ for spin up and down. The overall σ in front of the energy matrix appears due to the Nambu structure.[39,40] Here, we assume that the intraband impurity scattering, u_0 differs from the interband scattering between the bands separated by a large $\mathbf{Q}$, $u_{\mathbf{Q}}$. The Green's function (GF) matrix is obtained via $G_{\mathbf{k}\mathbf{k}'}(\tau) = -\langle T\hat{\psi}_{\mathbf{k}}(\tau)\hat{\psi}_{\mathbf{k}'}^{\dagger}(0)\rangle$, whence

$$G_{\mathbf{k}\mathbf{k}'}(\omega_n) = G_{\mathbf{k}}^0(\omega_n)[\delta_{\mathbf{k}\mathbf{k}'} + t_{\mathbf{k}\mathbf{k}'}(\omega_n)G_{\mathbf{k}'}^0(\omega_n)], \quad (4)$$

where $G_{\mathbf{k}}^0(\omega_n) = (i\omega_n - \hat{\beta}_{\mathbf{k}})^{-1}$ is the bare GF of the conduction electrons. Solving the Dyson equation for the T matrix

$$t_{\mathbf{k}\mathbf{k}'}(\omega_n) = \hat{U}_{\mathbf{k}\mathbf{k}'} + \sum_{\mathbf{k}''} \hat{U}_{\mathbf{k}\mathbf{k}''}G_{\mathbf{k}''}^0(\omega_n)t_{\mathbf{k}''\mathbf{k}'}(\omega_n), \quad (5)$$

the LDOS is obtained via analytic continuation $i\omega_n \to \omega + i\sigma 0^+$ according to

$$N^c(\omega, \mathbf{r}) = -\frac{1}{\pi} \mathrm{Im}\, \mathrm{Tr}[G(r, r, \omega_n)]_{i\omega_n \to \omega + i\sigma 0^+}. \quad (6)$$

We recall that the interference between incident and scattered waves gives rise to the spatial modulation of the amplitude of the total wave. This is then reflected in the LDOS. We further set $u_0 = 0.3t_\alpha$.

III. RESULTS

In what follows we discuss systematically the different ordered phases of the iron pnictides as shown in the phase diagram of Fig. 1 and present our calculated results for the total spectral function [Eqs. (4)–(6)]. The spectral function $\Sigma_\sigma \mathrm{Im}\, \mathrm{Tr}\, G_{0\sigma}(\mathbf{k}, \omega)$ of the clean system is always shown on the left panel. This allows to trace easily the most important scattering vectors that appear in the QPI corrections
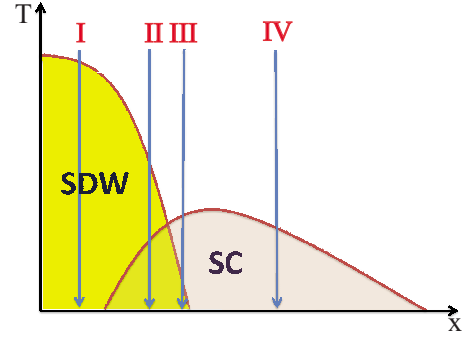

FIG. 1. (Color online) Schematic phase diagram for the iron-based superconductors $[\mathrm{Ba(Fe}_{1-x}\mathrm{Co}_x)_2\mathrm{As}_2$ and $\mathrm{SmFeAs(O}_{1-x}\mathrm{F}_x)]$ exhibiting a regime of coexistence of SDW and SC orders (Refs. 2 and 3). Regimes (I)–(IV) refer to the various parts of the phase diagram.

$\Sigma_{\mathbf{k}\sigma}\mathrm{Im}\,[G_{0\sigma}(\mathbf{k}, \omega)t_\sigma(\mathbf{k}, \mathbf{k}+\mathbf{q}, \omega)G_{0\sigma}(\mathbf{k}+\mathbf{q}, \omega)]$. We discuss the QPI maps for the case of nonmagnetic and magnetic impurities and show the difference between them. The latter is particular important for identifying the symmetry of the superconducting gap.

A. Spin-density wave phase

First, we review our results for the QPI in the SDW phase and its changes due to doping [regime (I) in Fig. 1] by showing in Figs. 2 and 3 the QPI for zero and 7% electron doping, respectively. A consequence of SDW order in parent iron-based superconductors is that the C_4 symmetry of the normal state is continuously broken. The resulting Fermi surface consists of small pockets which originate due to mixing of one of the hole pockets centered around the Γ point and the elliptic electron pocket centered around the $(0, \pi)$ point of the BZ as shown in the left panel. The scattering between the resulting boomeranglike structures (the most characteristic wave vectors $\mathbf{q}_1$ and $\mathbf{q}_2$ are indicated by arrows) dominates the QPI at low energies and occurs for both nonmagnetic and magnetic impurity scattering.[21,22]

Note that this reduction from C_4 to C_2 symmetry in the magnetically ordered state was originally interpreted as a sign of the underlying quasi-one-dimensional electronic structure and the electronic nematic order.[22,41] In our case, however, it appears just as a result of the translational symmetry-breaking induced by the $(0, \pi)$ antiferromagnetic state on the two-dimensional electronic structure. We also find that the C_4 symmetry is restored for bias energies exceeding twice the SDW gap value. Recently this prediction was confirmed experimentally[42] again signifying the dominant role of the magnetic order in breaking the C_4 symmetry.

For large enough W the FSs of the bands involved in the SDW are completely gapped and the same is true for the spectral densities at low energies. In this case, QPI will be determined by the bands which are not involved in the SDW, and, therefore, its structure will not show strong quasi-1D character. This may explain why the pure AF SDW state does not show any C_2-symmetric structure in the parent compounds where the magnetic moment (and the corresponding SDW gap) is quite large. Only when it is reduced upon dop-
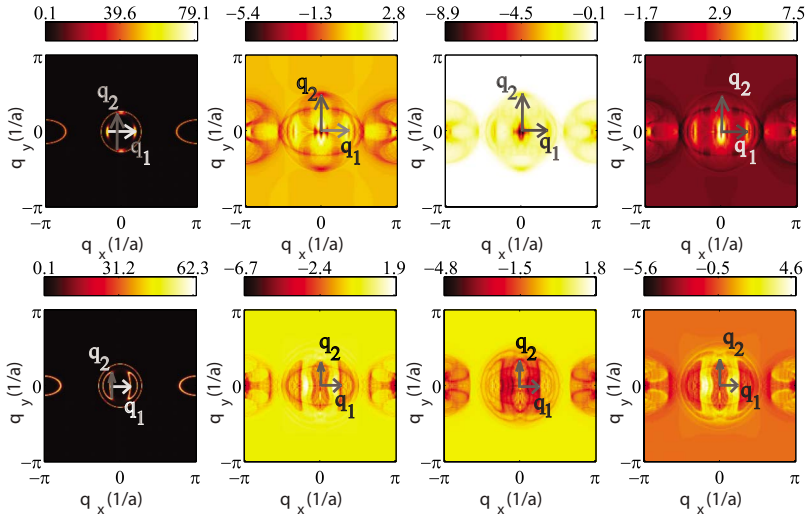
FIG. 2. (Color online) Constant energy intensity maps at $\omega=20$ meV (first row) and $w=-20$ meV (second row) of the spectral density, $\Sigma_\sigma \mathrm{Im}\, G_{0\sigma}(\mathbf{k},\omega)$, (first panel from the left) and QPI, $\Sigma_{\mathbf{k}\sigma} \mathrm{Im}\,[G_{0\sigma}(\mathbf{k},\omega)t_\sigma(\mathbf{k},\mathbf{k}+q,\omega)G_{0\sigma}(\mathbf{k}+q,\omega)]$ for nonmagnetic (second panel) and magnetic (third panel) impurities obtained as described in the text. The difference between QPI for nonmagnetic and magnetic impurities is displayed in the right panel. The color bars refer to the intensity in units of states/eV. The SDW order parameter is fixed at $W=40$ meV for zero doping.

ing, the bands involved in the SDW are located close to the FS so that the QPI structure, described above, becomes visible. Another apparent effect is the particle-hole asymmetry of the QPI which is the result of a rotation of the SDW-induced pockets from positive to negative energies by 90°. The asymmetry is 90° rotated in the case of electron doping (see Fig. 3). Due to the larger size of the electron pockets at $(\pm\pi,0)$ the SDW-induced small pockets are pronounced and dominate the scattering features in the QPI maps. For low negative energies the electron pocket is still present and the 90° rotation of the one-dimensional features shifts to lower energies.

B. Superconducting phase

Next, we discuss the QPI maps in the superconducting state. As mentioned above, the intensity of the QPI is affected by the relative sign of the order parameter between the FSs involved in the scattering via the Bogolyubov coherence factors representing the formation of Cooper pairs and new quasiparticles, which are coherent superpositions of electrons and holes. Coherence factors characterize how the scattering of a superconducting quasiparticle off a given scatterer differs from the scattering of a bare electron off the same scatterer. Generally, the momentum-dependent order-parameter enters into the expression for the coherence factor so that studies of scatterings of quasiparticles with different momenta can provide important information on the phase of the superconducting order parameter in momentum space. Originally, this idea was put forward for the cuprates.[43–45] In particular, for potential (nonmagnetic) scattering at wave vector $\mathbf{q}$ the corresponding coherence factor is smaller for those $\mathbf{q}$ which connect parts of the FS with the same sign of the SC gap.

Therefore, the QPI intensity appears only for sign-reversing momenta. In iron-based superconductors with s^{+-}-wave symmetry of the superconducting order parameter, this occurs for $(\pi,0)$ and $(0,\pi)$ momenta. Then for magnetic (time reversal) scattering, the QPI is negative for the wave vectors $(\pi,0)$ and $(0,\pi)$ and positive for momenta $(\pm\pi,\pm\pi)$ as the latter connects FSs with the same signs of the order parameter. Overall, the effect of the sign change of the superconducting gap can be most efficiently seen if one plots the difference of QPI for nonmagnetic and magnetic impurities.
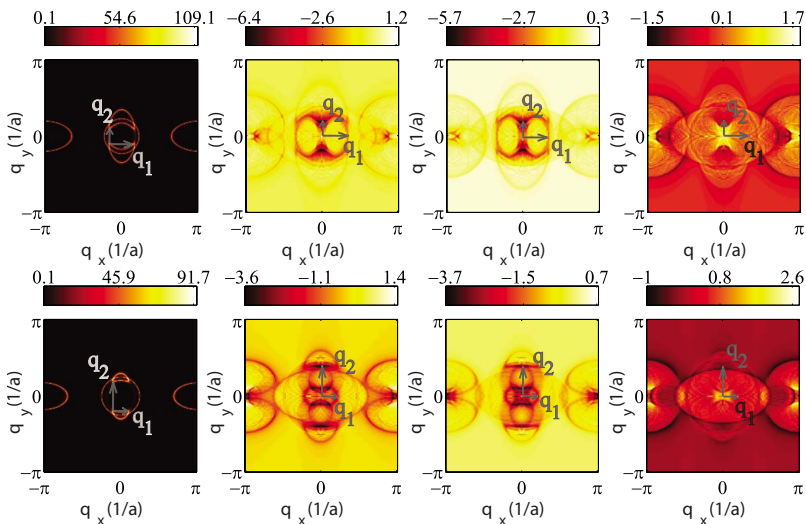

FIG. 3. (Color online) Constant energy intensity maps at $\omega=20$ meV (first row) and $w=-20$ meV (second row) of the spectral density and QPI, for nonmagnetic (second panel) and magnetic (third panel) impurities obtained as described in the text. The difference between QPI for nonmagnetic and magnetic impurities is displayed in the right panel. For SDW (region I in Fig. 1) with $W=40$ meV and with 7% electron doping (e-doping), for $\omega=20$ meV (first row) and $w=-20$ meV (second row). The color bars refer to the intensity in units of states/eV. The SDW order parameter is fixed at $W=40$ meV for 7% electron doping.
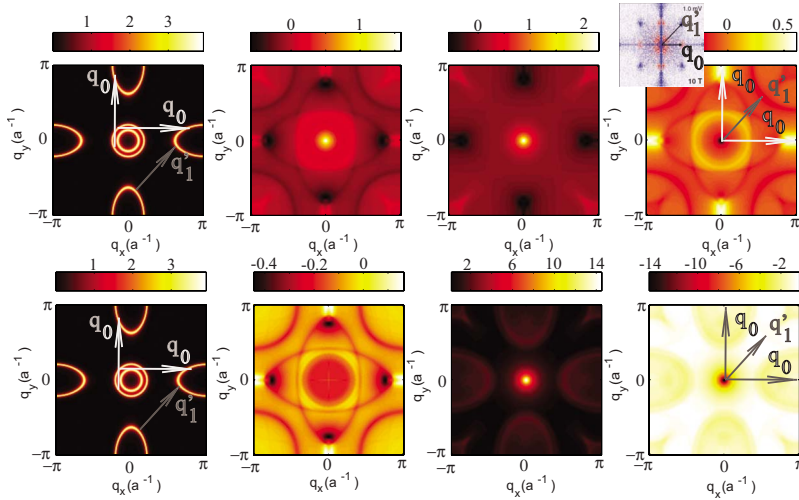
FIG. 4. (Color online) The spectral density and the QPI maps for nonmagnetic and magnetic impurity scattering (from left to right) at 20 meV in SC state with nodeless s^{+-} wave (upper panel) and isotropic s^{++}-wave (lower panel) symmetries of the superconducting gap. We set $\Delta = 20$ meV, 13% e-doping. The difference between QPI for nonmagnetic and magnetic impurities is displayed on the right panel. The arrows show scattering between electron and hole bands at $\mathbf{q}_0 = (\pi, 0)$, $(0, \pi)$. The inset in the upper panel shows the experimental data taken from Ref. 28.

As a result, a comparison of the QPI maps for magnetic and nonmagnetic scattering yields important information on the symmetry of the superconducting order parameter. In practice, the most straightforward way to perform this comparison in a type-II superconductor is to apply an external magnetic field where the resulting vortices act in part as magnetic scatterers.[28,44] Thus, by comparing the results with and without magnetic field the symmetry of the superconducting order can be deduced.

In Fig. 4 we show the QPI maps for the nodeless s^{+-} wave ($\Delta' = 0$) and isotropic s^{++}-wave symmetry. Clearly by subtracting the QPI for the nonmagnetic and magnetic scattering shown in the right panel, the difference between the two gaps becomes apparent with regard to the interband scattering (i) at $\mathbf{q}_0 = (\pm \pi, 0)$ or $(0, \pm \pi)$ which occurs for the scattering between electron and hole bands and (ii) diagonal $\mathbf{q}'_1$ scattering between two electron pockets. As the sign of the superconducting gap is opposite between the α and the β bands the difference in the QPI at $\mathbf{q}_0$ between nonmagnetic and magnetically induced scattering is positive. By contrast, that same difference in the scattering at $\mathbf{q}_1$ is negative as the order parameter on the electron pockets possesses the same sign. Both features are consistent with the QPI measured in the superconducting state of Fe(Se,Te) and Ba(Fe$_{1-x}$Co$_x$)$_2$As$_2$ compounds.[28,46] In particular, in the inset of Fig. 4 we show the SI-STM data taken at 10 T in FeTe$_{0.4}$Se$_{0.6}$ compound. Observe the difference in the intensities in the external magnetic field of 10 T for the scattering at $\mathbf{q}_0$ and $\mathbf{q}'_1$ which is consistent with our calculations. Note also that in the difference plot the details of the Fermi-surface scattering are very weakly visible, including the scattering between the electron pockets. Instead the largest effect occurs due the sign change of the gap and the corresponding coherence factors. For comparison, in Fig. 4 (lower panel) we show the same calculations for s^{++}-wave order parameter. The striking distinction with the s^{+-}-wave case is that the difference between nonmagnetic and magnetic impurity-induced QPI is, as expected, featureless.

In the next step we show the effect of higher harmonics in the s^{+-}-wave function. By taking a nonzero Δ', gap minima or even nodes form on the electron pockets. In this regard the evolution of the spectral density with energy will resemble

somewhat the structure found in nodal d-wave superconductors. In particular, due to the nodal structure of the superconducting gap, the spectral density with increasing energy will show a banana-shaped structure with new scattering momenta associated with the large density of states at the edges of the banana as shown in Fig. 5. We selectively show only some of the scattering wave vectors on this plot which we later identify on the QPI maps. Note that $\mathbf{q}'_1$ refers to the scattering with the same sign of the order parameter while other wavevectors, $\mathbf{q}'_2$, $\mathbf{q}'_3$, and $\mathbf{q}'_4$ connect regions with the superconducting order parameter of opposite sign. In principle, these additional features should be most pronounced in the difference of QPI intensities for magnetic and nonmagnetic scatterings.

The results for the spectral density and QPI maps are shown in Fig. 6. Due to relatively large quasiparticle lifetime
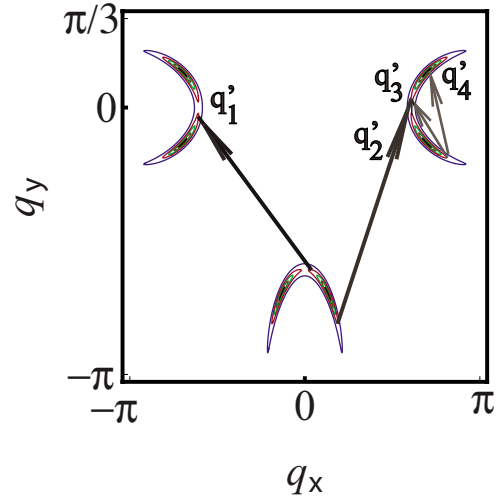

FIG. 5. (Color online) Calculated spectral density in the superconducting state with nodal s^{+-}-wave symmetry for $\Delta' = 3\Delta$. The arrows refer to some intraelectron and interelectron pocket scattering wave vectors (i.e., wavevectors joining regions with large DOS). Observe that $\mathbf{q}'_1$, and $\mathbf{q}'_2$, $\mathbf{q}'_3$, $\mathbf{q}'_4$ are the scattering wave vectors for the same and the opposite signs of the superconducting order parameter, respectively. The evolution of the banana-shape structures is shown for +5 (black curve), +10 (brown curve), +15 (green curve), +20 (red curve), and +30 (blue curve) meV.
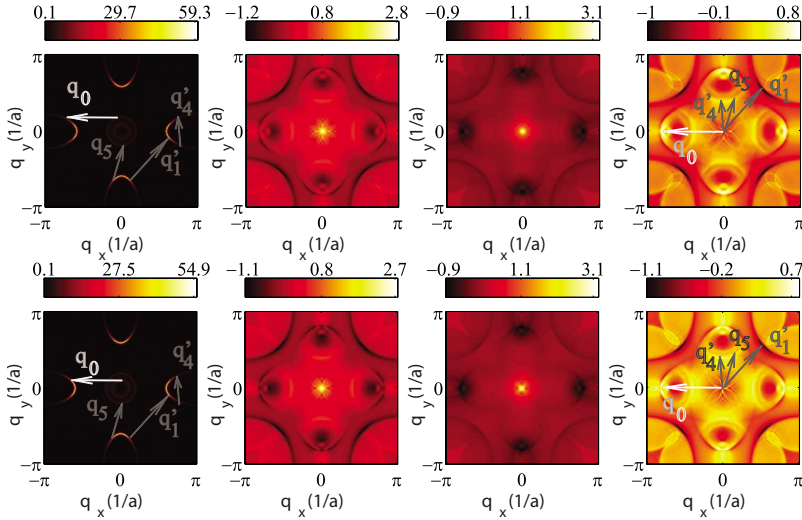
FIG. 6. (Color online) The spectral density and the QPI maps for nonmagnetic and magnetic impurity scattering (from left to right) at +20 meV (upper panel) and +10 meV (lower panel) in SC state with nodal s^{+-}-wave order parameter of the superconducting gap ($\Delta'=3\Delta$) and 13% of the electron doping. The difference between QPI for nonmagnetic and magnetic impurities is displayed on the right panel.

used in the calculations (~4 meV) the banana-shaped structures are not well resolved and overall the resulting QPI does not have well-defined momenta as those shown in Fig. 6. However, the anisotropy of the superconducting gap is clearly observed in the difference between magnetic and nonmagnetic impurity-induced QPI, as shown on the right panel. First, we again find the scattering along the diagonal momentum at $\mathbf{q}_1'$ which was also present in the case of a nodeless s^{+-}-wave symmetry. It is, however, additionally enhanced due to banana-shape structure and the corresponding high density of states at the edges of these bananas. Similarly, the interband-induced scattering between the α and the β bands (indicated by $\mathbf{q}_0$) acquires more structure. In addition, the maximum of intensity shifts from $(\pm\pi,0)$ and $(0,\pm\pi)$ to the smaller momenta due to the higher harmonics in the s^{+-}-wave gap. Additional peaks at small momenta include the scattering at $\mathbf{q}_4'$ within electron pockets and also the scattering between electron and hole pockets connecting states with opposite sign of the superconducting gap shown by $\mathbf{q}_5$. Overall, the structure of QPI becomes considerably richer, which should allow identification of the nodal structure of s^{+-}-wave superconducting order. One has to bear in mind, however, that the higher harmonics in the s^{+-}-wave

symmetry with corresponding scattering at $\mathbf{q}_4'$ and $\mathbf{q}_5$ should appear at larger doping. Note, to prove unambiguously whether these originate from the nodal s^{+-}-wave order-parameter measurements in an external magnetic field are required.

C. Coexistence phase with SDW and s^{+-} SC order

Finally, we consider the coexistence regime with both microscopic SDW and s^{+-}-wave superconducting order. In Fig. 7 we examine two different situations which correspond to regimes (II) and (III) of the phase diagram shown in Fig. 1, respectively. In regime (II) the SDW order parameter is larger than the SC one and we set $W=2\Delta$. In regime (III), which corresponds to higher doping, the situation reverses and we use $W=\Delta/2$. For the sake of simplicity and also because it is expected that the nodal s^{+-}-wave order occurs only at higher doping[37,47] we neglect the effect of the higher harmonics in the gap, i.e., we put $\Delta'=0$.

For the case of a larger SDW gap, the scattering has a pronounced C_2 symmetry and the only effect of superconductivity shown in the QPI, as compared to the pure SDW case, is to reduce the overall intensity of the scattering peaks
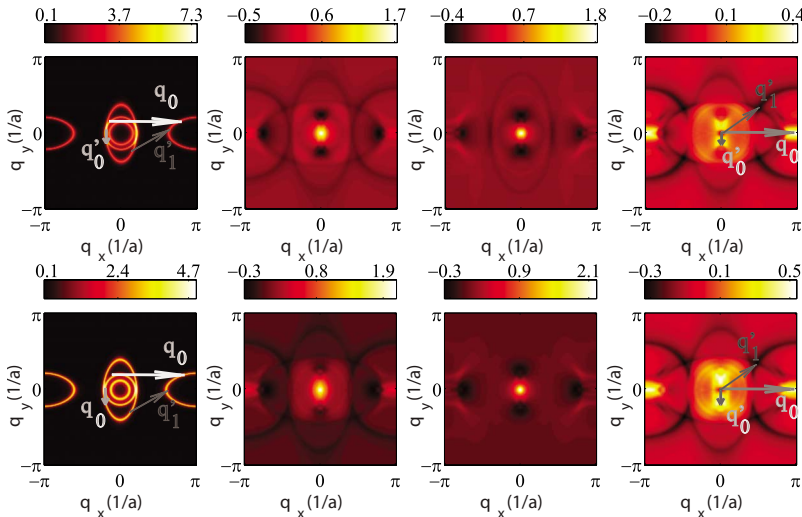

FIG. 7. (Color online) Calculated spectral density and the QPI maps at $\omega=+20$ meV in the coexistence regime of SDW+SC. The upper panel refers to the regime II of the phase diagram (Fig. 1) with $W=40$ meV, $\Delta=20$ meV and 10% e-doping. The lower panel describes the regime III with $W=10$ meV, $\Delta=20$ meV, and 12% e-doping.

(note the reduced intensity on the color bars). The latter occurs due to additional gapping of the bands. The structures visible in the upper panel of Fig. 7 are similar to those seen Fig. 2 with some extra smearing due to the superconducting gap. There are, however, additional structures which become particularly visible in the difference between QPI maps for magnetic and nonmagnetic scattering, which are signatures of the nodeless s^{+-}-wave gap. Note that these features strengthen in the case when the SC gap is larger than the SDW one, as is seen in the lower panel of Fig. 7.

The origin of these additional structures can be traced back to the effect of the SC s^{+-} order which is superimposed on the SDW order. First, notice that in the difference plot there is always an enhanced intensity at $\mathbf{q}_0=(\pm\pi,0)$ momenta. This is due to the fact that the electron and the hole band not involved in the SDW state with $(0,\pi)$ order have a different sign of the superconducting gap. Then for the very same reason as in the pure SC state with nodeless s^{+-}-wave order parameter, the difference between the magnetic and nonmagnetic impurity-induced QPI shows the strongest feature for interband scattering at $(\pm\pi,0)$ momenta. At the same time, new features arise due to the fact that one of the electron and one of the hole bands are mixed in the SDW state with $(0,\pi)$ ordering. However, both of these bands still possess an opposite sign of the superconducting gap, thus leading to a structure in the difference plot at small momenta. Remember that in the pure SC state with s^{+-}-wave order, these peaks would occur for $(0,\pm\pi)$ momentum but now this is a reciprocal wave vector of the SDW state. As a result, this scattering is "translated" to that around $q\sim0$ momentum. This clearly shows that the regime of microscopic coexistence of SDW+SC can be nicely observed in the FS-STM data. The same occurs for the scattering between two electron (β) bands. Originally along the diagonal of the BZ ($\mathbf{q}_1'$ in the nodeless s^{+-}-wave symmetry), it is now shifted to a different momentum due to the folding of the electron band involved in the SDW formation.

IV. CONCLUSION

In this paper we have systematically calculated quasiparticle interference effects due to magnetic and nonmagnetic impurities for the whole phase diagram of the iron pnictide superconductors. We have shown that in the SDW phase the QPI shows quasi-one-dimensional features as measured in recent experiments.[22] The C_4 symmetry is restored for energies larger than twice the SDW gap value. Furthermore, analyzing the superconducting state we have shown that the nodeless as well as the nodal s^{+-}-wave symmetry of the superconducting gap can be clearly identified in SI-STM experiments and distinguished from the isotropic s-wave gap. In particular, the scattering between the electron and the hole pockets at $\mathbf{q}_0=(\pm\pi,0)[(0,\pm\pi)]$ as well as the scattering between the electron pockets at $\mathbf{q}_1'$ becomes quite pronounced in the difference of the QPI maps between magnetic and nonmagnetic impurities, a feature found also in the experimental data.[28] We have demonstrated that a nontrivial angular dependence of the s^{+-}-wave gap induced by higher harmonics results in banana-shape structures in the QPI maps not present in the simplest version of s^{+-}-wave symmetry. A large density of states associated with the edges of these bananas is responsible for an additional low $\mathbf{q}$ scattering along the bond direction as well diagonal $\mathbf{q}$-scattering patterns in the QPI. Again these scatterings are especially pronounced in the difference plots between the magnetic and nonmagnetic impurity scattering. In the regime of coexistence of SDW and SC with s^{+-}-wave order our study has revealed additional characteristic features of the QPI which may help to identify this phase in iron-based superconductors. It includes: (a) the C_2 anisotropy of the QPI maps in the coexistence regime and (b) the low $\mathbf{q}$-interband scattering for the bands with opposite sign of the s^{+-} superconducting gap.

Note added: Recently the effect of the magnetic field on the QPI in an Iron-based superconductors was studied in Ref. 48. The results are in accordance with our findings.

[1] Y. Kamihara, T. Watanabe, M. Hirano, and H. Hosono, J. Am. Chem. Soc. **130**, 3296 (2008).

[2] Y. Laplace, J. Bobroff, F. Rullier-Albenque, D. Colson, and A. Forget, Phys. Rev. B **80**, 140501(R) (2009); M.-H. Julien, H. Mayaffre, M. Horvatic, C. Berthier, X. D. Zhang, W. Wu, G. F. Chen, N. L. Wang, and J. L. Luo, EPL **87**, 37001 (2009); C. Bernhard, A. J. Drew, L. Schulz, V. K. Malik, M. Rossle, C. Niedermayer, T. Wolf, G. D. Varma, G. Mu, H. H. Wen, H. Liu, G. Wu, and X. H. Chen, New J. Phys. **11**, 055050 (2009).

[3] F. Ning, K. Ahilan, T. Imai, A. S. Sefat, R. Jin, M. A. McGuire, B. C. Sales, and D. Mandrus, J. Phys. Soc. Jpn. **78**, 013711 (2009); C. Lester, J.-H. Chu, J. G. Analytis, S. C. Capelli, A. S. Erickson, C. L. Condron, M. F. Toney, I. R. Fisher, and S. M. Hayden, Phys. Rev. B **79**, 144523 (2009); D. K. Pratt, W. Tian,

A. Kreyssig, J. L. Zarestky, S. Nandi, N. Ni, S. L. Budko, P. C. Canfield, A. I. Goldman, and R. J. McQueeney, Phys. Rev. Lett. **103**, 087001 (2009).

[4] R. M. Fernandes, D. K. Pratt, W. Tian, J. L. Zarestky, A. Kreyssig, S. Nandi, M. G. Kim, A. Thaler, N. Ni, P. C. Canfield, R. J. McQueeney, J. Schmalian, and A. I. Goldman, Phys. Rev. B **81**, 140501(R) (2010).

[5] V. Cvetkovic and Z. Tesanovic, EPL **85**, 37002 (2009).

[6] A. V. Chubukov, D. V. Efremov, and I. Eremin, Phys. Rev. B **78**, 134512 (2008).

[7] I. Eremin and A. V. Chubukov, Phys. Rev. B **81**, 024511 (2010).

[8] A. B. Vorontsov, M. G. Vavilov, and A. V. Chubukov, Phys. Rev. B **81**, 174538 (2010).

[9] R. M. Fernandes and J. Schmalian, Phys. Rev. B **82**, 014521

(2010).

[10] D. J. Singh and M.-H. Du, Phys. Rev. Lett. **100**, 237003 (2008); L. Boeri, O. V. Dolgov, and A. A. Golubov, *ibid.* **101**, 026403 (2008); I. I. Mazin, D. J. Singh, M. D. Johannes, and M. H. Du, *ibid.* **101**, 057003 (2008).

[11] V. Barzykin and L. P. Gorkov, JETP Lett. **88**, 131 (2008).

[12] F. Wang, H. Zhai, Y. Ran, A. Vishwanath, and D.-H. Lee, Phys. Rev. Lett. **102**, 047005 (2009).

[13] M. M. Korshunov and I. Eremin, Phys. Rev. B **78**, 140509(R) (2008); EPL **83**, 67003 (2008).

[14] P. M. R. Brydon and C. Timm, Phys. Rev. B **79**, 180504(R) (2009).

[15] P. M. R. Brydon and C. Timm, Phys. Rev. B **80**, 174401 (2009).

[16] P. Brydon, M. Daghofer, and C. Timm, arXiv:1007.1949 (unpublished).

[17] R. Yu, K. T. Trinh, A. Moreo, M. Daghofer, J. A. Riera, S. Haas, and E. Dagotto, Phys. Rev. B **79**, 104510 (2009).

[18] M. D. Johannes and I. I. Mazin, Phys. Rev. B **79**, 220510(R) (2009); see also, Nat. Phys. **5**, 141 (2009).

[19] C. Platt, C. Honerkamp, and W. Hanke, New J. Phys. **11**, 055058 (2009).

[20] J. Knolle, I. Eremin, A. V. Chubukov, and R. Moessner, Phys. Rev. B **81**, 140506(R) (2010).

[21] J. Knolle, I. Eremin, A. Akbari, and R. Moessner, Phys. Rev. Lett. **104**, 257001 (2010).

[22] T.-M. Chuang, M. P. Allan, J. Lee, Y. Xie, N. Ni, S. L. Bud'ko, G. S. Boebinger, P. C. Canfield, and J. C. Davis, Science **327**, 181 (2010).

[23] K. McElroy, R. W. Simmonds, J. E. Hoffman, D.-H. Lee, J. Orenstein, H. Eisaki, S. Uchida, and J. C. Davis, Nature (London) **422**, 592 (2003).

[24] Q.-H. Wang and D.-H. Lee, Phys. Rev. B **67**, 020511(R) (2003).

[25] H. D. Chen, O. Vafek, A. Yazdani, and S. C. Zhang, Phys. Rev. Lett. **93**, 187002 (2004); K. Seo, H.-D. Chen, and J. Hu, Phys. Rev. B **76**, 020511(R) (2007); **78**, 094510 (2008).

[26] B. M. Andersen and P. J. Hirschfeld, Phys. Rev. B **79**, 144515 (2009).

[27] I. Paul, A. D. Klironomos, and M. R. Norman, Phys. Rev. B **78**, 020508(R) (2008).

[28] T. Hanaguri, S. Niitaka, K. Kuroki, and H. Takagi, Science **328**, 474 (2010).

[29] Y.-Y. Zhang, C. Fang, X. Zhou, K. Seo, W.-F. Tsai, B. A. Bernevig, and J. Hu, Phys. Rev. B **80**, 094528 (2009).

[30] E. Plamadeala, T. Pereg-Barnea, and G. Refael, Phys. Rev. B **81**, 134513 (2010).

[31] F. Wang, H. Zhai, and D.-H. Lee, Phys. Rev. B **81**, 184512 (2010).

[32] R. Thomale, Ch. Platt, J. Hu, C. Honerkamp, and B. A. Bernevig, Phys. Rev. B **80**, 180505 (2009).

[33] I. Mazin and D. Singh, arXiv:1007.0047 (unpublished).

[34] K. Kuroki, S. Onari, R. Arita, H. Usui, Y. Tanaka, H. Kontani, and H. Aoki, Phys. Rev. Lett. **101**, 087004 (2008).

[35] S. Graser, T. A. Maier, P. J. Hirschfeld, and D. J. Scalapino, New J. Phys. **11**, 025016 (2009); T. A. Maier, S. Graser, D. J. Scalapino, and P. J. Hirschfeld, Phys. Rev. B **79**, 224510 (2009).

[36] A. V. Chubukov, Physica C **469**, 640 (2009); V. Stanev, J. Kang, and Z. Tesanovic, Phys. Rev. B **78**, 184509 (2008)

[37] A. V. Chubukov, M. G. Vavilov, and A. B. Vorontsov, Phys. Rev. B **80**, 140515 (2009).

[38] A. V. Balatsky, I. Vekhter, and J.-X. Zhu, Rev. Mod. Phys. **78**, 373 (2006).

[39] Note, this definition of the Nambu spinor differs from the one used for the pure SDW state (Ref. 21), where $\hat{\psi}_{\mathbf{k}}^{\dagger} = (c_{\alpha_2\mathbf{k}\uparrow}^{\dagger}, c_{\alpha_1\mathbf{k}\uparrow}^{\dagger}, c_{\beta_1\mathbf{k}\uparrow}^{\dagger}, c_{\beta_2\mathbf{k}\uparrow}^{\dagger}, c_{\alpha_2\mathbf{k}\downarrow}^{\dagger}, c_{\alpha_1\mathbf{k}\downarrow}^{\dagger}, c_{\beta_1\mathbf{k}\downarrow}^{\dagger}, c_{\beta_2\mathbf{k}\downarrow}^{\dagger})$. This yields an opposite structure of the $\hat{\beta}_{\mathbf{k}}$ for the magnetic and nonmagnetic impurity.

[40] T. Hanaguri, C. Lupien, Y. Kohsaka, D.-H. Lee, M. Azuma, M. Takano, H. Takagi, and J. C. Davis, Nature (London) **430**, 1001 (2004).

[41] X. Zhou, C. Ye, P. Cai, X. Wang, X. Chen, and Y. Wang, arXiv:1008.2642 (unpublished).

[42] G. Li, X. He, A. Li, S. Pan, J. Zhang, R. Jin, A. Sefat, M. McGuire, D. Mandrus, B. Sales, and E. Plummer, arXiv:1006.5907 (unpublished).

[43] M. Maltseva and P. Coleman, Phys. Rev. B **80**, 144514 (2009).

[44] T. Hanaguri, Y. Kohsaka, M. Ono, M. Maltseva, P. Coleman, I. Yamada, M. Azuma, M. Takano, K. Ohishi, and H. Takagi, Science **323**, 923 (2009).

[45] T. Pereg-Barnea and M. Franz, Phys. Rev. B **78**, 020509(R) (2008).

[46] M. Teague, G. Drayna, G. Lockhart, P. Cheng, B. Shen, H. Wen, and N. Yeh, arXiv:1007.5086 (unpublished).

[47] R. Thomale, C. Platt, W. Hanke, and B. Andreibernevig, arXiv:1002.3599 (unpublished).

[48] S. Sykora and P. Coleman, arXiv:1010.3545 (unpublished).